HHS Public Access

Author manuscript

Eur J Nucl Med Mol Imaging. Author manuscript; available in PMC 2019 January 17.

Published in final edited form as:

Eur J Nucl Med Mol Imaging. 2014 October ; 41(10): 1879–1888. doi:10.1007/s00259-014-2791-x.

[^{18}F]Fluciclatide in the in vivo evaluation of human melanoma and renal tumors expressing $\alpha_v\beta_3$ and $\alpha_v\beta_5$ integrins

Esther Mena,
Molecular Imaging Program, NCI, NIH, Bethesda, MD, USA

Rikard Owenius,
GE Healthcare, Life Sciences, Uppsala, Sweden

Baris Turkbey,
Molecular Imaging Program, NCI, NIH, Bethesda, MD, USA

Richard Sherry,
Surgery Branch, NCI, NIH, Bethesda, MD, USA

Gennady Bratslavsky,
Urologic Oncology Branch, NCI, NIH, Bethesda, MD, USA

Sven Macholl,
GE Healthcare, Life Sciences, Amersham, UK

Matthew P. Miller,
GE Healthcare, Life Sciences, Amersham, UK

Ed J. Somer,
GE Healthcare, Life Sciences, Amersham, UK

Liza Lindenberg,
Molecular Imaging Program, National Cancer Institute, 10 Center Dr, MSC 1182, Bldg 10, Room B3B69, Bethesda, MD 20892-1088, USA

Stephen Adler,
Clinical Research Directorate/CMRP SAIC-Frederick Inc., NCI-Frederick, Bethesda, MD 21702, USA

Joanna Shih,
Biometric Research Branch, DCTD, NCI, NIH, Rockville, MD, USA

Peter Choyke, and
Molecular Imaging Program, NCI, NIH, Bethesda, MD, USA

Karen Kurdziel
Molecular Imaging Program, NCI, NIH, Bethesda, MD, USA

Correspondence to: Liza Lindenberg.

Disclosures

The authors Rikard Owenius, Sven Macholl, Matthew P. Miller, and Ed J. Somer are affiliated with GE Healthcare. The remaining authors have no conflicts of interest.

Abstract

Purpose—[^{18}F]Fluciclatide is an integrin-targeted PET radiopharmaceutical. $\alpha_v\beta_3$ and $\alpha_v\beta_5$ are upregulated in tumor angiogenesis as well as on some tumor cell surfaces. Our aim was to use [^{18}F]fluciclatide (formerly known as [^{18}F]AH111585) for PET imaging of angiogenesis in melanoma and renal tumors and compare with tumor integrin expression.

Methods—Eighteen evaluable patients with solid tumors ≥2.0 cm underwent [^{18}F]fluciclatide PET/CT. All patients underwent surgery and tumor tissue samples were obtained. Immunohistochemical (IHC) staining with mouse monoclonal antibodies and diaminobenzidine (DAB) was applied to snap-frozen tumor specimens, and additional IHC was done on formalin-fixed paraffin-embedded samples. DAB optical density (OD) data from digitized whole-tissue sections were compared with PET $SUV_{80\%\ max}$, and Patlak influx rate constant (K_i) data, tumor by tumor.

Results—Tumors from all 18 patients demonstrated measurable [^{18}F]fluciclatide uptake. At the final dynamic time-point (55 min after injection), renal malignancies (in 11 patients) demonstrated an average SUV80% max of 6.4±2.0 (range 3.8 – 10.0), while the average $SUV_{80\%\ max}$ for metastatic melanoma lesions (in 6 patients) was 3.0±2.0 (range 0.7 – 6.5). There was a statistically significant difference in [^{18}F]fluciclatide uptake between chromophobe and nonchromophobe renal cell carcinoma (RCCs, with $SUV_{80\%\ max}$ of 8.2± 1.8 and 5.4±1.4 (P= 0.020) and tumor-to-normal kidney (T/N) ratios of 1.5± 0.4 and 0.9±0.2, respectively (P=0.029). The highest Pearson's correlation coefficients were obtained when comparing Patlak K_i and $\alpha_v\beta_5$ OD when segregating the patient population between melanoma and RCC (r=0.83 for K_i vs. melanoma and r=0.91 for K_i vs. RCC). $SUV_{80\%\ max}$ showed a moderate correlation with $\alpha_v\beta_5$ and $\alpha_v\beta_3$ OD.

Conclusion—[^{18}F]Fluciclatide PET imaging was well tolerated and demonstrated favorable characteristics for imaging $\alpha_v\beta_3$ and $\alpha_v\beta_5$ expression in melanoma and RCC. Higher uptake was observed in chromophobe than in nonchromophobe RCC. [^{18}F]Fluciclatide may be a useful radiotracer to improve knowledge of integrin expression.

Keywords

$Alpha_v beta_3$ integrins; $Alpha_v beta_5$ integrins; [^{18}F]Fluciclatide; PET; Angiogenesis; Melanoma; Renal cell carcinoma

Introduction

Tumor-induced angiogenesis involves numerous signaling pathways mediated by growth factors, cellular receptors and adhesion molecules [1]. The integrins, $\alpha_v\beta_3$ and $\alpha_v\beta_5$, are cell adhesion molecules implicated in the formation of vascular endothelial cells and expressed on tumor cell surfaces [2]. They contain a specific peptide-binding pocket with high affinity attachment for the arginine-glycine-aspartate (RGD) tripeptide sequence [3]. Because they are expressed in abundance on the surface of angiogenic endothelial cells, these integrins and their binding ligand, RGD, are attractive targets for therapy and imaging.

The advance in antiangiogenic therapeutics has given impetus to the development of angiogenesis imaging agents. Various radiolabeled RGD ligands have been created for

integrin imaging [4, 5] but have not progressed as commercial products and therefore have limited availability in the clinic.

Renal cell cancer is the 12th most common cancer in the world and melanoma is the 19th according to the International Agency for Research on Cancer [6]. Melanoma is an aggressive malignancy and usually fatal with metastasis. Renal cell carcinoma (RCC) in the metastatic setting is similarly challenging with a poor prognosis. Angiogenesis is implicated in tumor growth and spread of many cancers, including melanoma and RCC and thus agents to disrupt this process have been tested in both diseases with great interest. Intetumumab and cilengitide, inhibitors of $\alpha_v\beta_3$ and $\alpha_v\beta_5$ integrins, have been studied in melanoma [7, 8]. Several antiangiogenic agents are used against metastatic RCC and include tyrosine kinase inhibitors, antivascular endothelial growth factor (VEGF) antibodies and mammalian target of rapamycin inhibitors. Many clinicians point to a need for functional imaging over anatomic imaging to accurately assess response to these therapies and this would benefit from an imaging tool targeting integrins [9].

The purpose of our study was to examine the ability of the integrin-targeting agent, [^{18}F]fluciclatide (formerly known as [^{18}F]AH111585), to detect and measure $\alpha_v\beta_3$ and $\alpha_v\beta_5$ expression in melanoma and RCC, diseases known to exhibit these integrins. To our knowledge, studies on these specific groups with this tracer have not been previously published. [^{18}F]Fluciclatide is a small synthetic cyclic peptide configured to bind with high affinity to the RGD binding site of $\alpha_v\beta_3$ and $\alpha_v\beta_5$ integrins [10]. We describe here the in vivo pharmacokinetics of [^{18}F]fluciclatide and evaluate the correlations of its uptake and retention with tissue biomarkers of integrin expression.

Materials and methods

Patient population and study design

This was a HIPAA-compliant, prospective, single-institution study, approved by the local Institutional Review Board. Inclusion criteria included adults who had been previously diagnosed with metastatic malignant melanoma, or primary or metastatic renal tumor, with a target tumor lesion >2.0 cm, scheduled for therapeutic resection or biopsy. Eighteen evaluable patients (7 women, 11 men; age 51±10 years, range 24 – 62 years) were examined with [^{18}F]fluciclatide PET/CT between 2009 and 2011, and all provided informed written consent. Following imaging, all patients were scheduled for surgery of the target lesion and the surgical specimens were sent for conventional histology and integrin immunohistochemistry (IHC). The demographic details of the patients and the imaging results are presented in Table 1.

[^{18}F]Fluciclatide PET/CT imaging

Of the 18 patients, 17 were imaged on a Philips Gemini TF PET/CT scanner in 3-D time of flight acquisition mode [11] and one was imaged on a GE LS Discovery scanner in 2-D acquisition mode. The images were reconstructed using the default row-action maximum-likelihood algorithm (RAMLA) iterative reconstruction and ordered-subsets expectation

maximization (OSEM), respectively [12], with standard corrections for randoms, scatter, attenuation, and normalization.

[^{18}F]Fluciclatide was synthesized by a commercial PET agent provider (Cardinal Health, Greenbelt, MD) under Good Manufacturing Practices (GMP) conditions according to previously published methods [13]. Blood samples were taken for analysis of preformed antibodies against fluciclatide prior to imaging – none was identified. No specific patient preparation was undertaken prior to imaging. Patients received a single bolus dose intravenous injection of [^{18}F]fluciclatide with a maximum total activity of 373.7 MBq (range 126.9 – 373.7 MBq). The estimated effective dose was approximately 26 μSv/MBq [14], resulting in a mean administered dose of 8.8 mSv.

The dynamic PET acquisition was initiated with a 30-s background frame, immediately after which the [^{18}F]fluciclatide was injected. The dynamic PET acquisition was performed for 60 min after injection (p.i.) with the target lesion within the field of view (FOV) using the following acquisition protocol (12 × 5-s frames, 6 × 10-s frames, 6 × 30-s frames, 5 × 2-min frames, 5 × 3-min, and 3 × 10-min frames). The patient was then taken off the scanner bed for a break and was encouraged to void. After voiding, the patient was repositioned on the scanner bed and a static torso PET acquisition (from the ears to the mid-thighs with 2 min per bed position) was initiated at about 80 min p.i. (range 71 – 91 min p.i.). Corresponding low-dose transmission CT scans (60 mA, 120 kVp) were acquired before each PET emission scan.

Image analysis

Images were prospectively assessed by two experienced nuclear medicine physicians, blinded to the histopathology results. For most of the eight patients with RCC, MRI images were also available and fused with the PET/CT images for improved anatomic correlation to tumor.

Only one lesion per subject, defined as the ‘target lesion’ was evaluated quantitatively. A volume of interest (VOI) was defined as the mean of the hottest 20 % of all pixels in the target lesion identified (80 % thresholded maximum standardized uptake value, $SUV_{80\%\ max}$) using MIM 5.2 (MIM Software, Cleveland, OH) and applied to the dynamic and static PET data. A VOI to estimate the blood pool was drawn manually as a spherical volume within a homogeneous location (>4 mm^3) within the largest vascular structure (typically the aorta) for the SUV_{BP} within the dynamic image FOV to estimate a vascular input function. Similarly, VOIs within the muscle (about 2.5 cm in diameter), and normal kidney parenchyma (>4 mm in diameter) contralateral to the tumor site were obtained to evaluate target lesions in relation to background uptake. The static $SUV_{80\%\ max}$ was obtained at 55 min p.i. because it is more representative of maximum radiotracer accumulation, based on previously published kinetics of [^{18}F]fluciclatide determined in a phase 1 study [10]. Tumor-to-blood (T/B) and tumor-to-muscle (T/M) ratios were also calculated at the same time-point.

Time–activity curves (TACs) representing $SUV_{80\%\ max}$ for each target lesion and SUV_{BP} were used in graphical analyses as described by Patlak and Blasberg [15] to assess

irreversible tracer binding. Image-derived blood curves (SUV_{mean}) were converted into metabolite-corrected plasma curves using group average curves of the plasma-to-blood ratio and percent intact radioligand calculations based on previous data with [^{18}F]fluciclatide [16]. These were used as subject-specific estimates of plasma input functions in the Patlak analysis. The SUV_{mean} attributable to the fractional blood volume in the tissue was estimated by linear least squares fitting for the first 2 min and then subtracted from the tissue SUV_{mean}. The tissue data corrected for fractional blood volume were fitted to a straight line for the time interval from 12 min (range 4.5 – 21 min) to 60 min. In the Patlak plot, the slope of the linear portion represents the tracer influx rate constant (K_i).

IHC analysis

The mean time between imaging and surgery (whole tumor resection) was 3.0 days (range 1 – 8 days). No attempt was made to coregister the specimen with the image. Instead, one single slice of each tumor was stained with each antibody. One set of specimens was snap-frozen in liquid nitrogen shortly after surgery and stored at −80 °C until thawed for staining. Another set of specimens from the same tumors were formalin-fixed paraffin-embedded (FFPE) shortly after surgery. All specimens underwent IHC after enrollment was closed, and were processed at the same time in the same laboratory. Standard hematoxylin and eosin staining was performed in the Pathology Department. IHC staining against integrins was performed at Huntingdon Life Sciences (Huntingdon, UK) following Good Clinical Practice (GCP) standards and using commercially available mouse monoclonal antibodies (Merck KGaA, Darmstadt, Germany): LM609 (0.05 μg/mL, titer 1:20,000) for $\alpha_v\beta_3$ integrin and P1F6 (0.2 μg/mL, titer 1:5,000) for $\alpha_v\beta_5$ integrin. The staining procedure included anti-mouse horseradish peroxidase and diaminobenzidine. Hematoxylin was employed as nuclear counterstain. Optimization and validation was undertaken on positive control tissues including melanoma and RCC specimens unrelated to this clinical study following the principles detailed by Bordeaux et al. [17]. Additional standard IHC staining of FFPE specimens against CD31 and VEGF, and all pathological analyses were performed at Clarient Inc. (Aliso Viejo, CA) in accordance with the principles of GCP. Digital whole-slide images were recorded on a MedMicro (Trestle Holdings Inc., Irvine, CA) slide scanning system and imported to the image analysis software Tissue Studio (Definiens AG, Munich, Germany) to calculate the optical density (OD) in tumor tissue regions. Each slide was assessed by a board-certified pathologist, with the main criteria being adequate tissue and staining quality and sufficient size of tumor regions. Then, up to four large ROIs (diameter typically of a few millimeters) were drawn in representative tumor tissue regions. The software performed a transformation to isolate the stain of interest (diaminobenzidine, brown stain), and calculated its OD. In parallel, images of smaller segments (tiles) of each ROI were automatically produced and manually inspected at higher magnification. Tiles with substantial artefacts or with predominantly nontumor tissue (e.g. stroma and high density of inflammation foci) were excluded. Finally, the tile OD results were averaged (weighted by tumor tissue area) to provide a single OD value per slide.

Statistical analysis

Descriptive statistics were used to summarize the PET data given as average±standard deviation (SD) $SUV_{80\%\ max}$ for melanomas and RCCs. The two-sample *t*-test was employed

to compare the differences in [^{18}F]fluciclatide uptake between chromophobe and nonchromophobe RCCs. A 95 % confidence interval was chosen to evaluate the differences between groups. Correlations between quantitative PET data and quantitative IHC variables were evaluated by linear regression analysis, calculating Pearson's correlation coefficient (r). The relationships among the different variables are also shown graphically. The level of significance was set at $P<0.05$.

Results

Clinical findings

[^{18}F]Fluciclatide injections were well tolerated by all patients without any radiotracer-related adverse events. One patient developed thrombocytopenia (<5,000 platelets/ml), which subsequently proved to be unrelated to [^{18}F]fluciclatide administration and was attributed to prior treatments. Anti-fluciclatide antibodies were negative. Histopathology was assessed in 18 tumor foci: six patients presented with metastatic malignant melanoma (Figs. 1 and 2), one patient had a large renal oncocytoma, ten patients had primary RCC (six nonchromophobe clear-cell carcinoma and four chromophobe-type; Fig. 3), and one patient had metastatic clear-cell (nonchromophobe) RCC within a large retroperitoneal lymph node.

All evaluable malignant target lesions (18 lesions) showed [^{18}F]fluciclatide tumor retention. The average lesion size in our population was 4.1 ± 1.7 cm (range 2.2 – 9 cm). There was no correlation between tumor size and [^{18}F]fluciclatide $SUV_{80\%\ max}$ uptake (r=0.35, P>0.05). Patients with renal malignancies showed increased [^{18}F]fluciclatide uptake with an average $SUV_{80\%\ max}$ of 6.4±2.0 (range 3.8 – 10.0), a T/B ratio of 1.5±0.4 and a T/M ratio of 8.5±3.4, whereas those with metastatic melanoma showed variable uptake with an average $SUV_{80\%\ max}$ of 3.0±2.0 (range 0.7 – 6.5), a T/B ratio of 0.7±0.4 and a T:M ratio of 4.5±3.9. Interestingly, the lowest $SUV_{80\%\ max}$ value (0.7) was obtained from a metastatic brain lesion, which showed low radiotracer uptake at earlier time points that increased with time, ultimately reaching an $SUV_{80\%\ max}$ of 1.54 at 125 min p.i. There was a statistically significant difference in [^{18}F]fluciclatide uptake between the four chromophobe RCCs and the seven nonchromophobe RCCs, with average $SUV_{80\%\ max}$ of 8.2±1.8 and 5.4±1.4, respectively (P=0.020). Given the high normal kidney parenchyma background uptake (average SUV_{mean} 5.8±1.3, range 3.6 – 7.5) due to the renal excretion of this agent [14], $SUV_{80\%\ max}$ of the kidney tumors was normalized to the normal kidney parenchyma background (T/N). This was also significantly higher for the chromophobe RCCs than in the nonchromophobe RCCs, with average T/N ratios of 1.5±0.4 and 0.9±0.2 (P=0.029). The renal oncocytoma showed an $SUV_{80\%\ max}$ of 9.20± 1.52, and a T/N ratio of 1.6.

Biodistribution and kinetics of [^{18}F]fluciclatide

All malignant tumors detected by the diagnostic standard reference (CT or MRI) were correctly identified on the [^{18}F]fluciclatide PET images, either as increases in radiotracer uptake compared with the surrounding normal tissue or as regions of visually reduced uptake because of the higher background, as in the nonchromophobe kidney tumors. High [^{18}F]fluciclatide uptake was observed in some normal organs such as the liver (average population SUV_{mean} 3.1 ±0.5, range 2.0 – 4.1). Low [^{18}F]fluciclatide uptake was seen in

muscle (average population SUV_{mean} 0.76±0.35, range 0.48 – 1.8), allowing a good tumor to background contrast in soft tissues and muscles. [^{18}F]Fluciclatide elimination is predominantly through the kidneys with variable bowel activity due to some hepatobiliary excretion.

Semiquantitative analysis

Mean tumor TACs (Fig. 4) showed rapid [^{18}F]fluciclatide uptake within the target tumors, peaking at approximately 2 – 3 min p.i. (blood flow), followed by a plateau from 10 min p.i.

The Patlak plots became linear from approximately 12 min p.i., suggesting that the binding kinetics can be interpreted as irreversible from the first hour of data. [^{18}F]Fluciclatide remained within the tumor even as the initial high concentration blood flow bolus equilibrated with the whole-body blood pool (Fig. 5). Patlak K_i was 0.0045±0.0026 min^{-1} (range 0.0014 – 0.0083 min^{-1}) in target melanomas and 0.0094±0.0047 min^{-1} (range 0.0049 – 0.0179 min^{-1}) for RCCs.K; from the Patlak plots correlated well (Pearson r=0.72) with the SUVs at 55 min. Pearson's r was lower for SUVs at earlier times (e.g. 12 and 28.5 min), confirming that the SUV at 55 min was more representative of the maximum rate of accumulation.

IHC and PET parameters

Overall, K_i was strongly correlated with $\alpha_v\beta_5$ expression in both melanomas (r=0.83) and RCCs (r=0.91), and moderately correlated with $\alpha_v\beta_3$ expression in both melanomas (r=0.53) and RCCs (r=0.42; Fig. 6).Semiempirical $SUV_{80\%\ max}$ was moderately correlated with both $\alpha_v\beta_3$ and $\alpha_v\beta_5$ expression in both melanomas (r=0.63 for $\alpha_v\beta_5$ and r= 0.40 for $\alpha_v\beta_3$) and RCCs (r=0.50 for $\alpha_v\beta_5$ and r=0.44 for $\alpha_v\beta_5$). Correlations of PET parameters with CD31 microvessel density (MVD) and with VEGF OD were inconsistent across specimens and overall no significant correlation was seen.

Discussion

This study demonstrated the feasibility and tolerability of [^{18}F]fluciclatide PET imaging in patients with metastatic melanoma or kidney tumors. Our data corroborated the findings of previous studies in humans with [^{18}F]fluciclatide [10], showing favorable tumortargeting properties, including rapid and high tumor uptake, quick clearance from blood and normal tissues, and high T/M ratios, resulting in favorable image contrast and tumor delineation.

Clinical PET studies with [^{18}F]fluciclatide were initially performed in healthy volunteers to assess safety, radiation dosimetry and biodistribution [14], and later in patients with breast or lung cancer to evaluate kinetic modeling and estimate tumor/background specific binding [10, 18]. In our cohort, a high detection rate was found, identifying all tumors (in 18 patients) consistent with previous results in which all 18 lesions in seven patients with advanced metastatic breast cancer were detected by [^{18}F]fluciclatide PET imaging [10]. The malignant lesions in our cohort of patients showed heterogeneous tracer uptake with an average $SUV_{80\%\ max}$ of 6.8 ± 3.2 that was independent of tumor size. [^{18}F]Fluciclatide showed significantly higher radiotracer uptake in chromophobe than in nonchromophobe RCCs, with average $SUV_{80\%\ max}$ of 8.2± 1.8 and 5.4±1.4 (P=0.020) and average T/N ratios

of 1.5±0.4 and 0.9±0.2 (P=0.029), respectively. Distinguishing between the two RCC types is significant in terms of patient prognosis and therapeutic options. $\alpha_v\beta_3$ integrin expression also showed a strong correlation with $SUV_{80\%\ max}$ in chromophobe and nonchromophobe RCC (r = 0.93 and r = 0.002; P=0.066). The high r value for the correlation between $SUV_{80\%\ max}$ and $\alpha_v\beta_3$ may have been due to the small sample of patients with chromophobe RCC (four patients). Surprisingly high uptake ($SUV_{80\%\ max}$ 9.20, T/N ratio 1.7) was seen in the single oncocytoma. This is interesting because previous research has suggested a histopathological link between renal oncocytoma and chromophobe RCC [19]. In the single patient with brain metastases, [^{18}F] fluciclatide retention was not found in normal brain but was localized in tumor at the site of disruption of the blood–brain barrier–a finding also reported with [^{18}F]galacto-RGD in patients with glioblastoma [20].

The ability of [^{18}F]fluciclatide to target the neovasculature via the $\alpha_v\beta_3$ and $\alpha_v\beta_5$ integrins expressed on endothelial cells was initially reported by Pasqualini et al. [21], who demonstrated that tumor endothelial cells are targeted by the RGD sequence. Subsequent imaging studies focused mostly on $\alpha_v\beta_3$ while we chose to additionally measure $\alpha_v\beta_5$ expression. This was supported by an in vitro study [10] showing that fluciclatide binding is about two orders of magnitude stronger to $\alpha_v\beta_5$ than to $\alpha_v\beta_3$. A significant correlation between $\alpha_v\beta_3$ expression and radiotracer uptake with [^{18}F]galacto-RGD PET was later demonstrated in murine tumor models [22, 23] and in melanoma and sarcoma patients (r=0.94, P=0.005) [24]. Beer et al. [25] also evaluated $\alpha_v\beta_3$ expression in both tumors and tumor-associated vasculature, and showed excellent correlations (Spearman's R=0.92, P<0.0001) between $\alpha_v\beta_3$ expression and uptake of [^{18}F]galacto-RGD in subjects with a variety of different tumor types. IHC markers of angiogenesis, such as staining intensity of $\alpha_v\beta_3$ and MVD, have been shown to correlate well with tumor retention of [^{18}F]galacto-RGD on endothelial cells and on tumor cells of breast cancer patients [26] and head and neck carcinomas [27]. Beer et al. [25] used a semiquantitative method of correlation expressing staining intensity as 0, +1, +2 or +3. In the current study, a quantitative rather than semiquantitative IHC analysis was performed using continuous OD measurements as described by Spector et al. [28] yielding similar but less highly correlated results. This could have been due to artifacts from processing or limited sampling of tumor as will be discussed below.

Positive strong to moderate correlations were observed between each of the PET parameters (K_i, and $SUV_{80\%\ max}$) and $\alpha_v\beta_5$ and $\alpha_v\beta_3$ expression in patients with metastatic melanoma and renal tumors. For renal tumors, these correlations were seen in samples of both chromophobe and nonchromophobe tumors. The strongest correlation was seen with chromophobe carcinomas between K; and $\alpha_v\beta_3$, which are usually highly vascular tumors, but are less common than clear-cell (nonchromophobe) carcinomas of the kidney. This observation has potential therapeutic implications for the use of anti-integrin agents in chromophobe carcinomas.

Regarding melanoma, our results are concordant with those of previously published preclinical and clinical studies that showed high levels of $\alpha_v\beta_3$ integrin expression in melanoma [29, 30], contrary to lower integrin expression levels reported in RCC [31,25].

There are some potential limitations of this study. First, we studied a small number of patients. Nonetheless, the observed difference in uptake between chromophobe and nonchromophobe renal tumors was sufficient to achieve significance. Second, we employed digital histopathology of whole-tissue sections rather than more subjective readings of smaller FOVs, hoping for better reproducibility. Third, IHC of frozen sections is susceptible to artefacts due to tissue processing and freeze-thaw damage, potentially reducing the expected correlation between integrin expression and IHC positivity. Fourth, we employed a single IHC slide per tumor from a random position within the tumor rather than probing multiple sites or the site of greatest [^{18}F]fluciclatide uptake. Fifth, the single IHC slides and the PET images were not spatially coregistered, and hence the IHC slide may not be representative of the site of highest [^{18}F]fluciclatide uptake. Finally, we did not measure MVD, therefore we could not estimate the contribution of integrin measured in the tumor vasculature to integrin uptake in the entire tumor.

The next promising application of [^{18}F]fluciclatide PET imaging would be to determine its utility in monitoring the status of $\alpha_v\beta_3$ and $\alpha_v\beta_5$ expression before and during antiangiogenic therapies [32]. A number of antiangiogenic agents are now approved for use or are in late phase clinical trials [33–36].

Conclusion

The favorable imaging and tolerability characteristics of [^{18}F]fluciclatide allowed feasible visualization of target tumors with high tumor-to-background ratios in melanoma and RCC, and [^{18}F]fluciclatide uptake showed strong to moderate correlation with integrin expression on IHC. Our data suggestthat [^{18}F]fluciclatide is a promising, novel PET radiotracer that could improve knowledge of integrin expression in solid tumors. Larger studies are needed to explore its full potential.

Acknowledgments

We thank Adrian Smith, Derek Grant, Brian Higley and Ian Wilson from GE Healthcare, and Tanya Ledezma and Karen Yamamoto for support. We also thank Earl Henry for consultancy with the statistical analyses. This trial was sponsored by GE Healthcare.

References

1. Angiogenesis Folkman J.. Annu Rev Med. 2006;57:1–18. doi:10.1146/annurev.med.57.121304.131306. [PubMed: 16409133]
2. Desgrosellier JS, Cheresh DA. Integrins in cancer: biological implications and therapeutic opportunities. Nat Rev Cancer. 2010;10(1):9–22. [PubMed: 20029421]
3. Ruoslahti E, Pierschbacher MD. New perspectives in cell adhesion: RGD and integrins. Science. 1987;238(4826):491–7. [PubMed: 2821619]
4. Haubner R, Wester HJ. Radiolabeled tracers for imaging of tumor angiogenesis and evaluation of anti-angiogenic therapies. Curr PharmDes. 2004;10(13):1439–55.
5. Gaertner FC, Kessler H, Wester HJ, Schwaiger M, Beer AJ. Radiolabelled RGD peptides for imaging and therapy. Eur J Nucl Med Mol Imaging. 2012;39 Suppl 1:S126–38. doi:10.1007/s00259-011-2028-1. [PubMed: 22388629]
6. Ferlay J, Soerjomataram I, Ervik M, Dikshit R, Eser S, Mathers C, et al. GLOBOCAN 2012 v1.0, Cancer Incidence and Mortality Worldwide: IARC CancerBase No. 11. Lyon: International Agency for Research on Cancer; 2013 Available from: http://globocan.iarc.fr. Accessed 29 May 2014.

7. Kim KB, Prieto V, Joseph RW, Diwan AH, Gallick GE, Papadopoulos NE, et al. A randomized phase II study of cilengitide (EMD 121974) in patients with metastatic melanoma. Melanoma Res. 2012;22(4):294–301. doi:10.1097/CMR.0b013e32835312e4. [PubMed: 22668797]
8. O'Day S, Pavlick A, Loquai C, Lawson D, Gutzmer R, Richards J, et al. A randomised, phase II study of intetumumab, an anti-alphav-integrin mAb, alone and with dacarbazine in stage IV melanoma. Br J Cancer. 2011;105(3):346–52. doi:10.1038/bjc.2011.183. [PubMed: 21750555]
9. Bex A, Fournier L, Lassau N, Mulders P, Nathan P, Oyen WJ, et al. Assessing the response to targeted therapies in renal cell carcinoma: technical insights and practical considerations. Eur Urol. 2014;65(4): 766–77. doi:10.1016/j.eururo.2013.11.031. [PubMed: 24341958]
10. Kenny LM, Coombes RC, Oulie I, Contractor KB, Miller M, Spinks TJ, et al. Phase I trial of the positron-emitting Arg-Gly-Asp (RGD) peptide radioligand 18F-AH111585 in breast cancer patients. JNucl Med. 2008;49(6):879–86. doi:10.2967/jnumed.107.049452. [PubMed: 18483090]
11. Surti S, Kuhn A, Werner ME, Perkins AE, Kolthammer J, Karp JS. Performance of Philips Gemini TF PET/CT scanner with special consideration for its time-of-flight imaging capabilities. J Nucl Med Off Publi Soc Nucl Med. 2007;48(3):471–80.
12. Browne J, de Pierro AB. A row-action alternative to the EM algorithm for maximizing likelihood in emission tomography. IEEE Trans Med Imaging. 1996;15(5):687–99. doi:10.1109/42.538946. [PubMed: 18215950]
13. Glaser M, Morrison M, Solbakken M, Arukwe J, Karlsen H, Wiggen U, et al. Radiosynthesis and biodistribution of cyclic RGD peptides conjugated with novel [18F]fluorinated aldehyde-containing prosthetic groups. Bioconjug Chem. 2008;19(4):951–7. doi:10.1021/bc700472w. [PubMed: 18341272]
14. McParland BJ, Miller MP, Spinks TJ, Kenny LM, Osman S, Khela MK, et al. The biodistribution and radiation dosimetry of the Arg-Gly-Asp peptide 18F-AH111585 in healthy volunteers. J Nucl Med. 2008;49(10):1664–7. doi:10.2967/jnumed.108.052126. [PubMed: 18794263]
15. Patlak CS, Blasberg RG. Graphical evaluation of blood-to-brain transfer constants from multiple-time uptake data. Generalizations. J Cereb Blood Flow Metab. 1985;5(4):584–90. [PubMed: 4055928]
16. Ringheim AM, Miller MP, Owenius R. 18F-fluciclatide (RGD peptide) PET in metastatic breast cancer: impact of labeled metabolites on Patlak analysis and qualification of the use of image-derived blood input. Eur J Nucl Med Mol Imaging. 2012;39(2):498–611. doi:10.1007/s00259-012-2225-6.
17. Bordeaux J, Welsh A, Agarwal S, Killiam E, Baquero M, Hanna J, et al. Antibody validation. Biotechniques. 2010;48(3):197–209. doi: 10.2144/000113382. [PubMed: 20359301]
18. Tomasi G, Kenny L, Mauri F, Turkheimer F, Aboagye EO. Quantification of receptor-ligand binding with [18F]fluciclatide in metastatic breast cancer patients. Eur J Nucl Med Mol Imaging. 2011;38(12):2186–97. doi:10.1007/s00259-011-1907-9. [PubMed: 21892622]
19. Yusenko MV. Molecular pathology of renal oncocytoma: a review. Int J Urol. 2010;17(7):602–12. doi:10.1111/j.1442-2042.2010.02574.x. [PubMed: 20590944]
20. Schnell O, Krebs B, Carlsen J, Miederer I, Goetz C, Goldbrunner RH, et al. Imaging of integrin alpha(v)beta(3) expression in patients with malignant glioma by [18F] Galacto-RGD positron emission tomography. Neuro Oncol. 2009;11(6):861–70. doi:10.1215/15228517-2009-024. [PubMed: 19401596]
21. Pasqualini R, Koivunen E, Ruoslahti E. Alpha v integrins as recep-tors for tumor targeting by circulating ligands. Nat Biotechnol. 1997;15(6):542–6. doi:10.1038/nbt0697-542. [PubMed: 9181576]
22. Haubner R, Wester HJ, Weber WA, Mang C, Ziegler SI, Goodman SL, et al. Noninvasive imaging of alpha(v)beta3 integrin expression using 18F-labeled RGD-containing glycopeptide and positron emission tomography. Cancer Res. 2001;61(5):1781–5. [PubMed: 11280722]
23. Zhang X, Xiong Z, Wu Y, Cai W, Tseng JR, Gambhir SS, et al. Quantitative PET imaging of tumor integrin alphavbeta3 expression with 18F-FRGD2. JNucl Med. 2006;47(1):113–21. [PubMed: 16391195]
24. Haubner R, Weber WA, Beer AJ, Vabuliene E, Reim D, Sarbia M, et al. Noninvasive visualization of the activated alphavbeta3 integrin in cancer patients by positron emission tomography and

[18F]Galacto-RGD. PLoS Med. 2005;2(3):e70. doi:10.1371/journal.pmed.0020070. [PubMed: 15783258]

25. Beer AJ, Haubner R, Sarbia M, Goebel M, Luderschmidt S, Grosu AL, et al. Positron emission tomography using [18F]Galacto-RGD identifies the level of integrin alpha(v)beta3 expression in man. Clin Cancer Res. 2006;12(13):3942–9. doi:10.1158/1078-0432.ccr-06-0266. [PubMed: 16818691]
26. Beer AJ, Niemeyer M, Carlsen J, Sarbia M, Nahrig J, Watzlowik P, et al. Patterns of alphavbeta3 expression in primary and metastatic human breast cancer as shown by 18F-Galacto-RGD PET. J Nucl Med. 2008;49(2):255–9. doi:10.2967/jnumed.107.045526. [PubMed: 18199623]
27. Beer AJ, Grosu AL, Carlsen J, Kolk A, Sarbia M, Stangier I, et al. [18F]galacto-RGD positron emission tomography for imaging of alphavbeta3 expression on the neovasculature in patients with squamous cell carcinoma of the head and neck. Clin Cancer Res. 2007;13(22 Pt 1):6610–6. doi: 10.1158/1078-0432.ccr-07-0528. [PubMed: 18006761]
28. Spector NL, Xia W, Burris H, 3rd, Hurwitz H, Dees EC, Dowlati A, et al. Study of the biologic effects of lapatinib, a reversible inhibitor of ErbB1 and ErbB2 tyrosine kinases, on tumor growth and survival pathways in patients with advanced malignancies. J Clin Oncol. 2005;23(11):2502–12. doi:10.1200/jco.2005.12.157. [PubMed: 15684311]
29. Seftor RE, Seftor EA, Hendrix MJ. Molecular role(s) for integrins in human melanoma invasion. Cancer Metastasis Rev. 1999;18(3):359–75. [PubMed: 10721490]
30. McGary EC, Lev DC, Bar-Eli M. Cellular adhesion pathways and metastatic potential of human melanoma. Cancer Biol Ther. 2002;1(5):459–65. [PubMed: 12496470]
31. Wechsel HW, Petri E, Feil G, Nelde HJ, Bichler KH, Loesr W. Renal cell carcinoma: immunohistological investigation of expression of the integrin alpha v beta 3. Anticancer Res. 1999;19(2C):1529–32. [PubMed: 10365138]
32. Cai J, Han S, Qing R, Liao D, Law B, Boulton ME. In pursuit of new anti-angiogenic therapies for cancer treatment. Front Biosci (Landmark Ed). 2011;16:803–14. [PubMed: 21196204]
33. Battle MR, Goggi JL, Allen L, Barnett J, Morrison MS. Monitoring tumor response to antiangiogenic sunitinib therapy with 18F-fluciclatide, an 18F-labeled alphaVbeta3-integrin and alphaV beta5-integrin imaging agent. J Nucl Med. 2011;52(3):424–30. doi:10.2967/jnumed. 110.077479. [PubMed: 21321268]
34. Morrison MS, Ricketts SA, Barnett J, Cuthbertson A, Tessier J, Wedge SR. Use of a novel Arg-Gly-Asp radioligand, 18F-AH111585, to determine changes in tumor vascularity after antitumor therapy. JNucl Med. 2009;50(1):116–22. doi:10.2967/jnumed.108.056077. [PubMed: 19091899]
35. Sun X, Yan Y, Liu S, Cao Q, Yang M, Neamati N, et al. 18F-FPPRGD2 and 18F-FDG PET of response to Abraxane therapy. J Nucl Med. 2011;52(1):140–6. doi:10.2967/jnumed.110.080606. [PubMed: 21149494]
36. Jin ZH, Furukawa T, Claron M, Boturyn D, Coll JL, Fukumura T, et al. Positron emission tomography imaging of tumor angiogenesis and monitoring of antiangiogenic efficacy using the novel tetrameric peptide probe 64Cu-cyclam-RAFT-c(-RGDfK-)4. Angiogenesis. 2012;15(4):569–80. doi:10.1007/s10456-012-9281-1. [PubMed: 22644563]

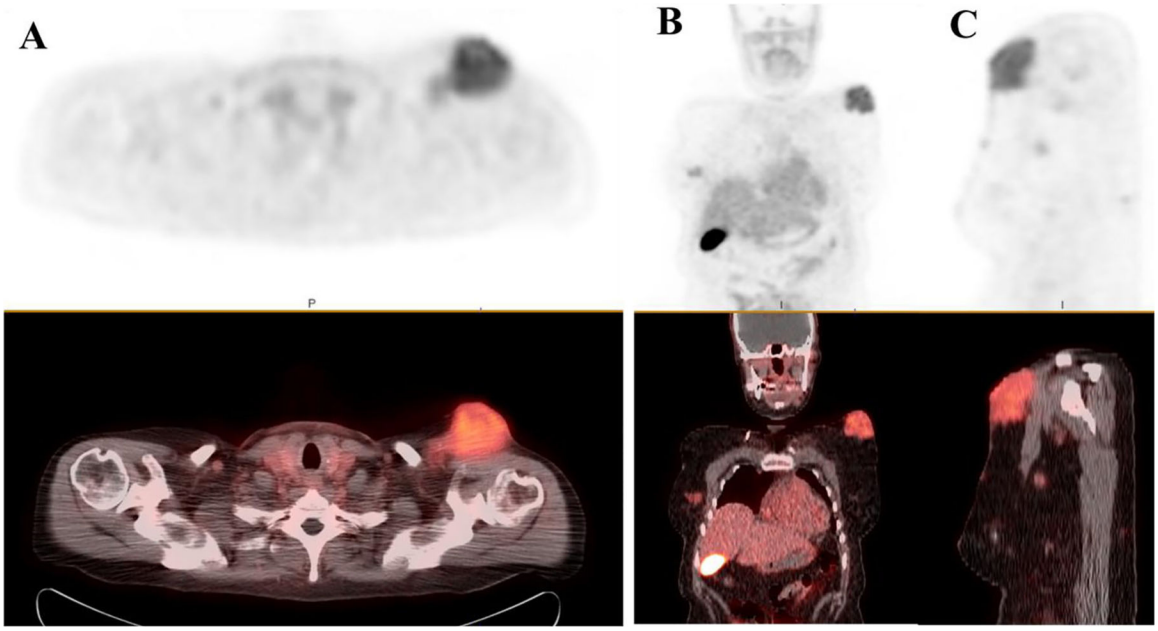

Fig. 1.

[^{18}F]Fluciclatide PET/CT images in patient 4 (malignant melanoma.) Axial (**a**) sagittal (**b**) and coronal (**c**) images show focal radiotracer uptake within a left supraclavicular mass, with $SUV_{80\%\ max}$ 6.5, as well as in other soft tissue nodules

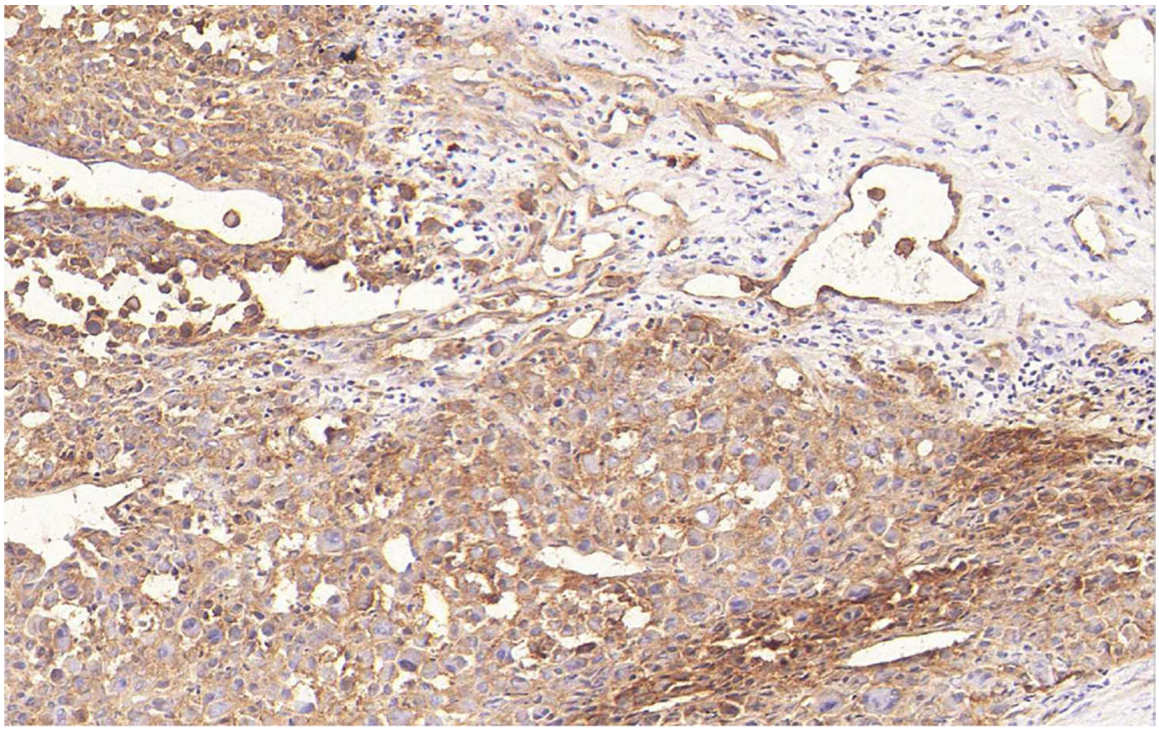

Fig. 2.

Section of resected melanoma tissue from patient 4. Diaminobenzidine staining against $\alpha_v\beta_3$ is seen predominantly in the cytoplasm but also in the membranes of tumor cells. Staining intensity in the stroma is low as expected

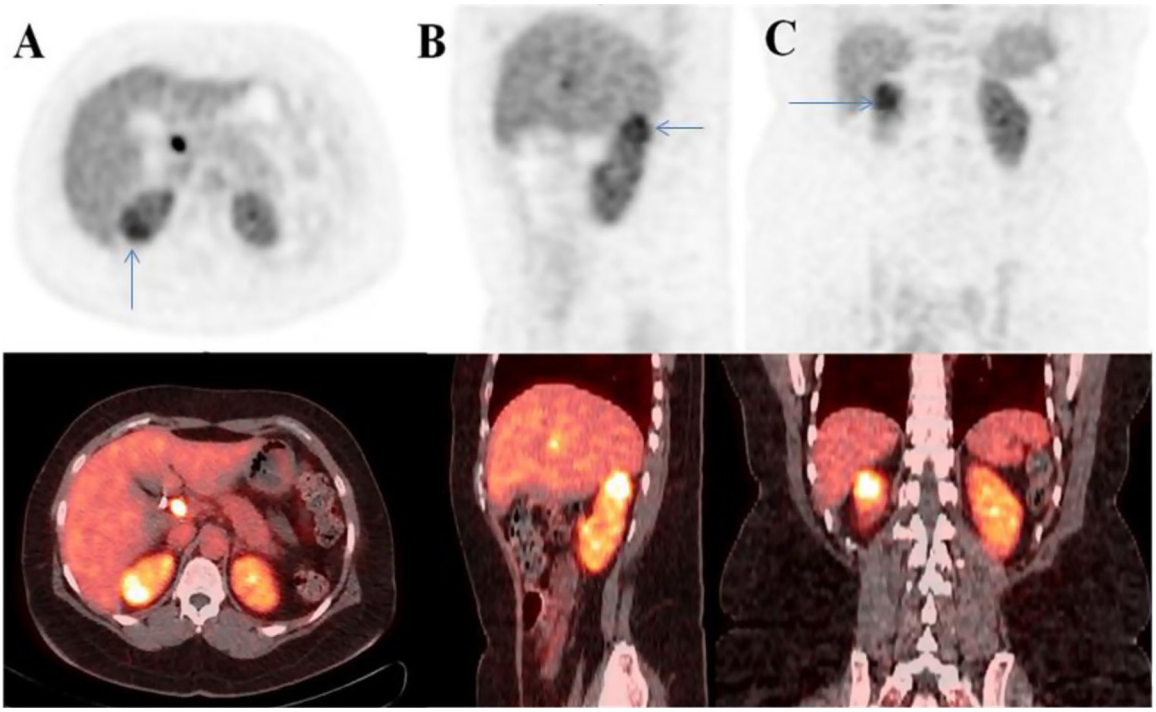

Fig. 3.

[^{18}F]Fluciclatide PET/CT images of a right kidney tumor (*arrows*) in patient 10. Axial (**a**), sagittal (**b**) and coronal (**c**) images show abnormally increased uptake of [^{18}F]fluciclatide within the tumor ($SUV_{80\%\ max}$ 8.9). A renal tumor with a chromophobe component was confirmed by pathology

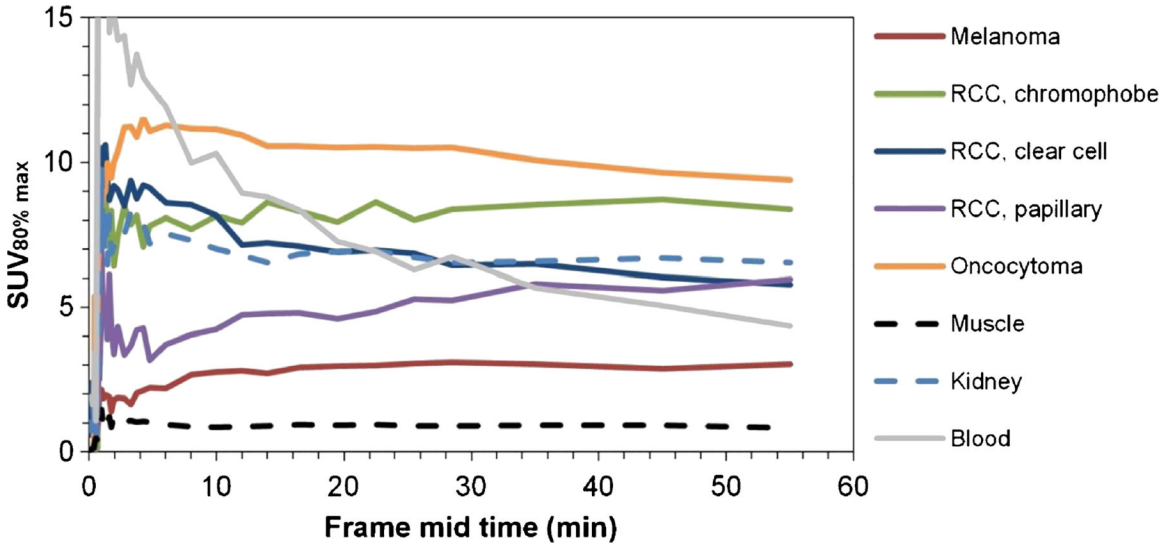

Fig. 4.

Mean TACs for target lesions (group averages of $SUV_{80\%\ max}$ for the different cancer types), normal tissues (SUV_{mean} for muscle and kidney) and arterial blood (SUV_{mean})

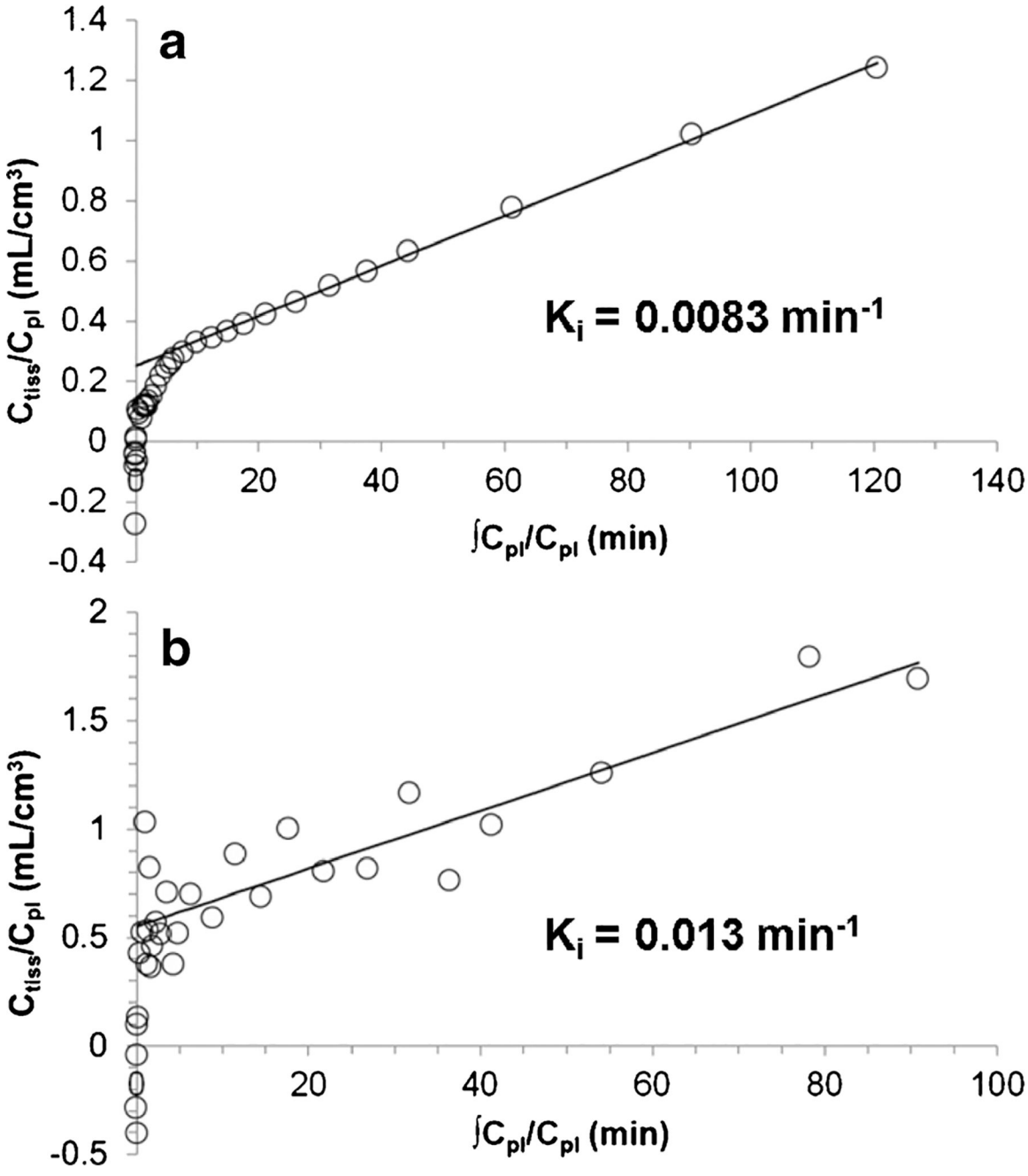

Fig. 5.

Patlak plots obtained from TACs representing $SUV_{80\%\ max}$ of target lesions (**a** melanoma in patient 4. **b** RCC with chromophobe component in patient 10). K_i is given by the slope of the linear curve fitted to the data. C_{pl} and C_{tiss} represent the activity concentrations in plasma and tissue, respectively

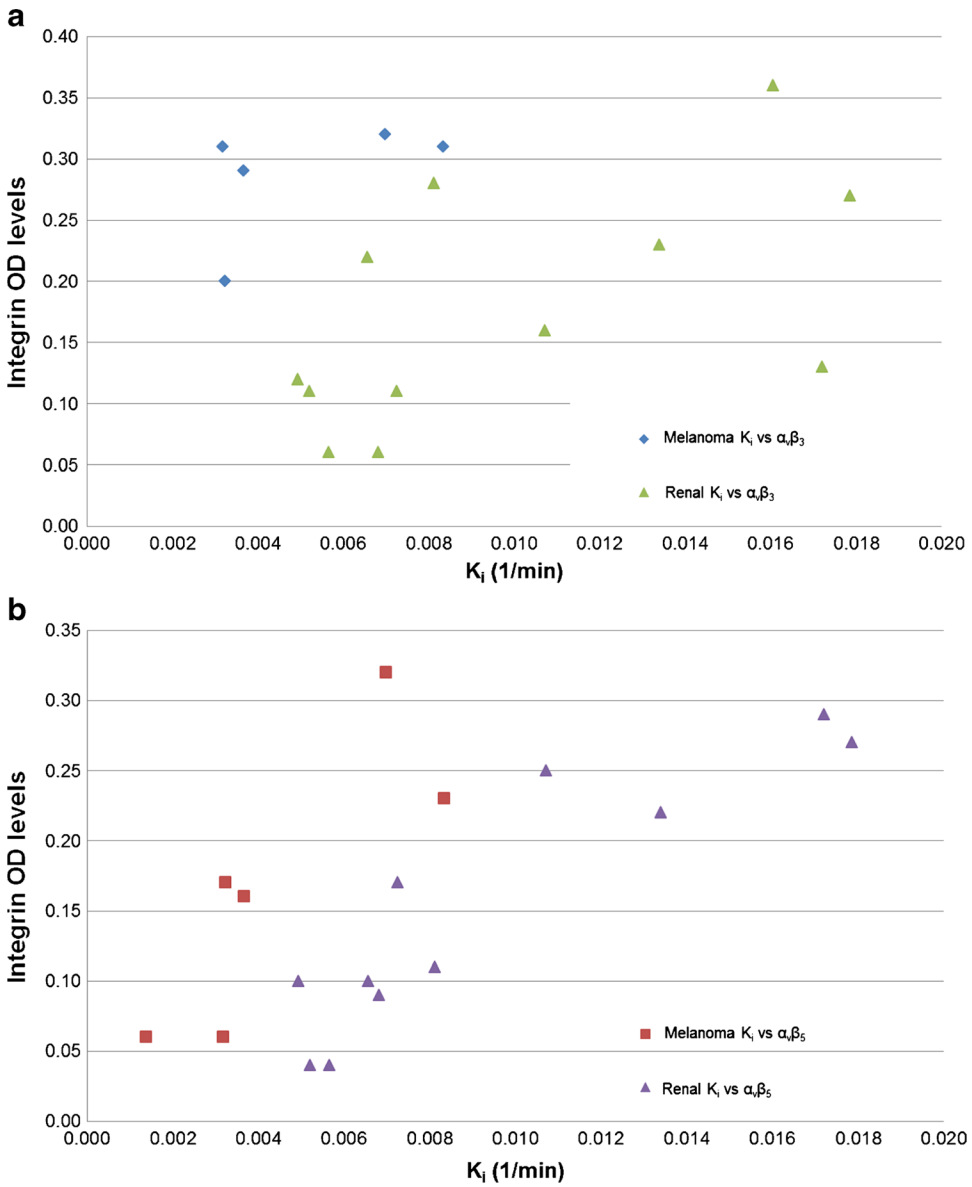

Fig. 6.

Correlation plots of K_i vs. $\alpha_v\beta_3$ (**a**) and $\alpha_v\beta_5$ (**b**). The strongest correlation is seen between K_i and the $\alpha_v\beta_5$ integrin OD levels in both melanomas and RCCs

Table 1

Patient demographics and results

Patient	Age (years)	Sex	Diagnosis	Target lesion		[^{18}F]Fluciclatide $SUV_{80\%\ max}$	Uptake ratios		K_i	Immunohistochemistry	
				Location	Size (cm)		Tumor-to-blood	Tumor-to-muscle		$\alpha_v\beta_3$	$\alpha_v\beta_5$
1	36	F	Metastatic melanoma	Small-bowel jejunum	2.6	3.7	0.7	4.8	0.0037	0.29	0.16
2	32	F	Metastatic melanoma	Upper back soft tissue	4.1	1.8	0.6	2.8	0.0032	0.31	0.06
3	57	M	Metastatic melanoma	Left occipital	2.5	0.7	0.2	0.8	0.0014	Not measured	0.06
4	49	F	Metastatic melanoma	Left supraclavicular	4.1	6.5	1.4	12	0.0083	0.31	0.23
5	56	F	Metastatic melanoma	Left axilla	4.5	3.3	0.9	4	0.0070	0.32	0.32
6	59	M	Metastatic melanoma	Anterior chest wall	2.6	2.1	0.4	2.6	0.0032	0.20	0.17
7	62	M	Oncocytoma	Left kidney	9.0	9.2	2.7	11	0.016	0.36	0.14
8	54	F	RCC, chromophobe	Left kidney	3.8	8.1	1.6	8.7	0.011	0.16	0.25
9	57	M	RCC, chromophobe	Right kidney	3.1	5.8	1.9	7.6	0.017	0.13	0.29
10	50	F	RCC, chromophobe	Right kidney	3.1	8.9	1.6	12.8	0.013	0.23	0.22
11	60	M	RCC, chromophobe	Right kidney	5.2	10.0	2.6	11.6	0.018	0.27	0.27
12	56	M	RCC, clear cell	Left kidney	3.6	6.1	1.2	3.4	0.0052	0.11	0.04
13	57	M	RCC, clear cell	Right kidney	3.5	6.5	1.3	6.3	0.0066	0.22	0.10
14	48	M	RCC, clear cell	Right kidney	3.2	7.8	1.4	13.6	0.0049	0.12	0.10
15	47	M	RCC, clear cell	Retroperitoneal	5.0	4.5	1.3	9.4	0.0073	0.11	0.17
16	53	M	RCC, clear cell, metastatic	Left kidney	5.6	3.8	1.1	3.7	0.0068	0.06	0.09
17	24	F	RCC, clear cell	Left kidney	3.6	4.2	1.1	6.1	0.0081	0.28	0.11
18	59	M	RCC, papillary	Right kidney	6.8	5.0	1.3	10.3	0.0057	0.06	0.04